UNIVERSITY of York

This is a repository copy of *Novel Electrically Excited Doubly Salient Variable Reluctance Machine with High-order-harmonic Winding*.

White Rose Research Online URL for this paper:
https://eprints.whiterose.ac.uk/199728/

Version: Accepted Version

Article:
Ni, Feifan, Niu, Shuangxia, Li, Zhenghao et al. (1 more author) (2023) Novel Electrically Excited Doubly Salient Variable Reluctance Machine with High-order-harmonic Winding. IEEE Transactions on Magnetics. ISSN 1941-0069

https://doi.org/10.1109/TMAG.2023.3279887

Reuse
This article is distributed under the terms of the Creative Commons Attribution (CC BY) licence. This licence allows you to distribute, remix, tweak, and build upon the work, even commercially, as long as you credit the authors for the original work. More information and the full terms of the licence here: https://creativecommons.org/licenses/

Takedown
If you consider content in White Rose Research Online to be in breach of UK law, please notify us by emailing eprints@whiterose.ac.uk including the URL of the record and the reason for the withdrawal request.

White Rose university consortium
Universities of Leeds, Sheffield & York

eprints@whiterose.ac.uk
https://eprints.whiterose.ac.uk/

This article has been accepted for publication in IEEE Transactions on Magnetics. This is the author's version which has not been fully edited and content may change prior to final publication. Citation information: DOI 10.1109/TMAG.2023.3279887

Novel Electrically Excited Doubly Salient Variable Reluctance Machine with High-order-harmonic Winding

Feifan Ni[1], Shuangxia Niu [1], *Senior Member IEEE* , Zhenghao Li[1] and Xing Zhao[2]

[1]Department of Electrical Engineering, The Hong Kong Polytechnic University, Hong Kong, 999077
[2]School of Physics, Engineering and Technology, The University of York, York YO10 5DD, UK

DC excited doubly salient variable reluctance machine has received more attention due to its robust rotor structure, low cost and permanent magnet-free. In this paper, a short-pitch distributed winding connection with improved fifth order harmonic is newly applied in this kind of machine to enhance the torque production under the same current excitation. Its electromagnetic performance is analyzed by finite element analysis. The simulation results verify that compared with the traditional concentrated winding distribution, the proposed winding arrangement can effectively improve the back EMF as well as the motor output torque density.

***Index Terms*—Flux modulation, high-order-harmonic winding, stator field winding, Variable reluctance machine (VRM).**

I. Introduction

With the rising price of permanent magnets, more environmentally friendly motors without permanent magnets are gaining more and more attention for its low cost and robustness although motors with permanent magnets have already been used in a large number of industrial applications[1]-[4].

Typical PM-free motors include synchronous reluctance motors (SynRMs), switched reluctance motors (SRM), etc. Synchronous reluctance machine has the same stator design as the conventional permanent magnet motor, but its torque density and power factor are lower that limit its application in industry [5]. SRM motors have significant torque ripple and mechanical vibration due to the half-cycle conductivity principle. Since the SRM drive circuit is an asymmetric half-bridge converter, commercial inverter cannot be used [6].

To overcome these disadvantages, some new motor structures have been proposed, such as DC excited variable reluctance machine (DC-VRMs). It has simple rotor structure compared to SynRMs which means DC-VRM has better mechanical strength [7]. It also achieves much lower torque ripple than that of SRMs at the same time. However, these DC-VRMs have full DC coil structure resulting in higher DC copper losses in the motor and the DC coil occupies a larger slot area [8]-[14].

In this paper, a novel electrically excited doubly salient variable reluctance machine (DC-DSVRM) with a DC coil spanning three stator teeth is investigated. Compared to existing doubly salient machine, it has a symmetrical magnetic circuit and sinusoidal back EMF to reduce torque ripple. It shows comparable torque density but reduced DC copper losses compared to DC-VRMs using full DC coils. To further enhance the torque density of the motor, an armature winding configuration that based on the flux modulation theory is proposed in this paper. Compared to the conventional winding design, this novel armature winding configuration can fully utilize the higher order harmonics generated by field winding based on its unique distribution in doubly salient machine, thus increasing the motor's back EMF and the torque density.

The rest of this paper is organized as follows. In Section II, the machine structure of the novel electrically excited doubly salient variable reluctance machine and working principle are introduced with the analyze of the air-gap harmonic. In Section III, the novel armature winding design is given based on the flux modulation theory and the feasibility is verified. In Section IV, the model with conventional armature winding and the novel winding design are established and the electromagnetic performance are compared. Finally, the conclusion is drawn in Section V.

II. Machine Structure and Working Principle

A. Machine Structure

In this paper, an 18-stator slot and 13-rotor pole DC-DSVRM is analyzed. In the stator, both dc field winding and ac armature winding are housed. The dc field coils, which are wound across every three stator teeth, can produce the flux density of fundamental harmonic and other higher order harmonics.

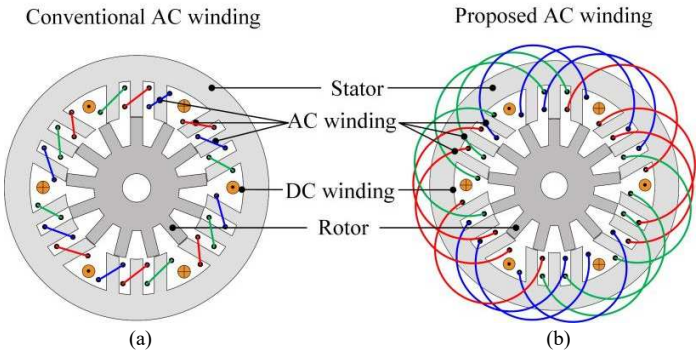

Fig. 1. Winding connection of 18/13 DC-DSVRM with dc field coils across three stator teeth. (a) Model I concentrated winding design. (b) Model II distributed winding design.

In the existing doubly salient machines, concentrated armature winding connections are usually utilized in the conventional design. In this paper, a distributed winding design utilizing working harmonics modulated from high-order-harmonics is proposed and compared with the conventional design. Two models with different armature windings are showed in Fig.1. For convenience, the model

Authorized licensed use limited to: University of York. Downloaded on May 30,2023 at 13:00:08 UTC from IEEE Xplore. Restrictions apply.
© 2023 IEEE. Personal use is permitted, but republication/redistribution requires IEEE permission. See https://www.ieee.org/publications/rights/index.html for more information.

This article has been accepted for publication in IEEE Transactions on Magnetics. This is the author's version which has not been fully edited and content may change prior to final publication. Citation information: DOI 10.1109/TMAG.2023.3279887

with conventional concentrated winding is named Model I, and the model with proposed distributed winding is named Model II.

The dimensions of both models are optimized using GA algorithms and finite element methods to obtain larger torque and lower torque pulsation while fixing the stator outer radius and rotor inner radius. The main parameters for the DC-DSVRMs are denoted in Fig.2. The values of these parameters are listed in Table I.

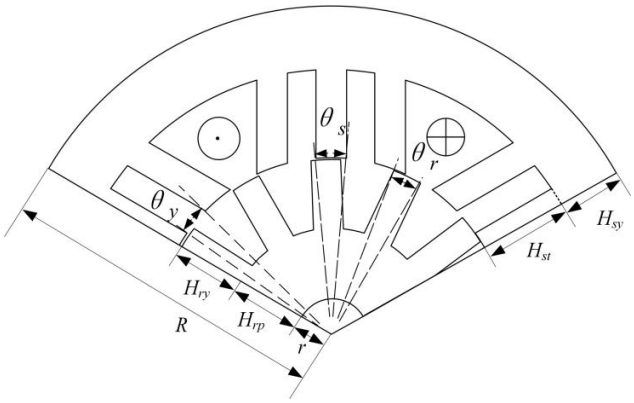

Fig. 2. Illustration of 18/13 DC-DSVRM.

TABLE I
MAIN PARAMETERS OF THE DC-DSVRM

Parameters	Notation	Model I	Model II
Number of stator slots	N_s	18	18
Number of rotor slots	N_r	13	13
Rotation speed (rpm)	v_r	60	60
Stack length(mm)	L	80	80
Rotor inner Radius(mm)	r	10	10
Stator outer Radius(mm)	R	100	100
Armature winding coil turns	n_{ac}	51	62
Field winding coil turns	n_{dc}	187	206
Armature current(A)	I_{ac}	5.7	5.7
Field current (A)	I_{dc}	4	4
Stator yoke height(mm)	H_{sy}	20.1	12.8
Stator yoke width(deg)	θ_y	10.18	10.48
Stator tooth height(mm)	H_{st}	28.9	30.2
Stator tooth width(deg)	θ_s	9.5	9.18
Rotor yoke height(mm)	H_{ry}	11.8	26.8
Rotor pole height(mm)	H_{rp}	28.7	19.7
Rotor pole width(deg)	θ_r	14.48	10.82
Air-gap length(mm)	δ	0.5	0.5

B. Working Principle and Harmonic Distribution

In order to prove the feasibility of the novel winding, the field generated by the dc field coils which are wound across three stator teeth is studied with a simple airgap MMF and permeability model. The 1-D model of the DC-DSVRM is established as Fig.2.

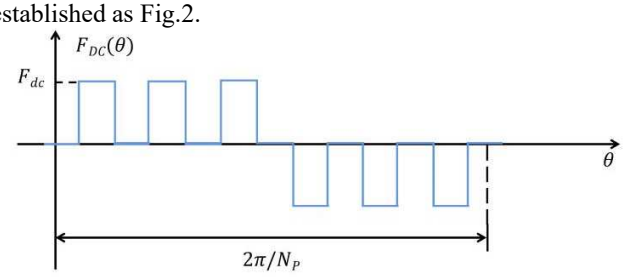

Fig. 3. MMF waveform of DC field winding.

To simplify the calculation, we assume that the permeability of the stator and rotor cores is infinite, and ignore the effect of flux leakage.

Fig.3 shows the MMF waveform generated by the dc field taking the midpoint of the stator slot where the DC winding is placed as the origin. θ_s is the angle of the stator tooth, F_{dc} is the amplitude of the MMF across effective air gap. Since the DC coils are wound across three stator teeth, the fundamental pole pair number (PPN) of DC excitation is calculated as (1),

$$N_p = \frac{N_s}{6} \tag{1}$$

where N_s is the number of stator slots, which equals to 18.

According to Fourier transform theory, the MMF of DC field winding can be expressed as follows.

$$F_{dc}(\theta) = \sum_{n=1}^{+\infty} F_n \sin\left(nN_p\theta\right) \tag{2}$$

$$F_n = \frac{2}{\pi}\int_0^{\pi} F_{dc}(\theta)\sin\left(nN_p\theta\right)d\theta \quad n = 1,2,3\ldots \tag{3}$$

where F_n is the Fourier coefficient, n is a positive integer number. Furtherly, we can obtain the expression for F_n as follows,

$$F_n = -\frac{4F_{dc}}{nN_p\pi}\sin\left(\frac{nN_p\theta_s}{2}\right)\left[\sin\left(\frac{n\pi}{3}-\frac{nN_p\theta_s}{2}\right)\right. \\ \left.+\sin\left(n\pi-\frac{3nN_p\theta_s}{2}\right)+\sin\left(\frac{5n\pi}{3}-\frac{5nN_p\theta_s}{2}\right)\right] \tag{4}$$

where $n\,(n = 1,2,3\ldots)$ is the order of harmonics, θ is the air-gap position, and θ_s is the angle of slot opening.

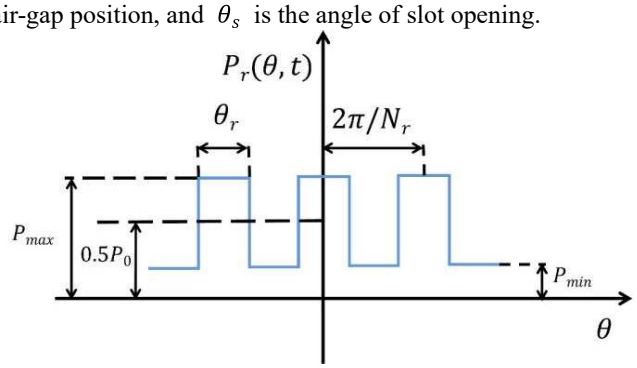

Fig. 4. Rotor permeance waveform.

The MMF of DC field winding is then modulated by the rotor teeth whose waveform is shown in Fig.4 The rotor permeance waveform can be expressed by the equation (5).

$$\begin{cases} P_r(\theta,t) = \frac{P_0}{2} + \sum_{k=1}^{+\infty} P_k\cos[kN_r(\theta-\omega t)] \\ P_0 = 2P_{min} + \frac{(P_{max}-P_{min})\theta_r N_r}{\pi} \\ P_k = \frac{2}{k\pi}(P_{max}-P_{min})\sin\left(kN_r\frac{\theta_r}{2}\right) \end{cases} \tag{5}$$

where P_{max} is the permeance of rotor salient poles, P_{min} is the permeance of rotor slots, N_r is the number of rotor salient poles, ω is the mechanical angular speed of the rotor, and θ_2 is the mechanical angle of the rotor salient pole. $\frac{P_0}{2}$ represents the DC component of the MMF.

Multiplying the expression for MMF with the expression for rotor permeance yields the air gap flux density,

$$B_r(\theta,t) = F_{DC}(\theta)P_r(\theta,t) \\ = \sum_{n=1}^{+\infty}\sum_{k=-\infty}^{+\infty}\frac{F_nP_{|k|}}{2}\sin\left(nN_p\theta + kN_r\theta - kN_r\omega t\right) \tag{6}$$

Authorized licensed use limited to: University of York. Downloaded on May 30,2023 at 13:00:08 UTC from IEEE Xplore. Restrictions apply.
© 2023 IEEE. Personal use is permitted, but republication/redistribution requires IEEE permission. See https://www.ieee.org/publications/rights/index.html for more information.

This article has been accepted for publication in IEEE Transactions on Magnetics. This is the author's version which has not been fully edited and content may change prior to final publication. Citation information: DOI 10.1109/TMAG.2023.3279887

According to the expression of the air gap flux density, the PPN of each harmonic component can be obtained. Due to the magnetic modulation theory, the air-gap flux density consists many space harmonic components whose PPN can be divided into three groups, nN_p, $nN_p + kN_r$, $nN_p - kN_r$, respectively. The order and the speed of each harmonic component group are shown in TABLE II.

TABLE II SPACE HARMONIC COMPONENTS OF FLUX DENSITY

Group	Harmonic pole-pair number	Speed
I	nN_p	0
II	$nN_p + kN_r$	$\frac{kN_r}{nN_p + kN_r}\omega$
III	$nN_p - kN_r$	$\frac{kN_r}{\lvert nN_p - kN_r \rvert}\omega$

The first group is not modulated by the rotor and remains stationary. Thus it can not be utilized as working harmonics. The second and third group are modulated by the rotor poles which means some of them can be chosen as working harmonics.

III. ARMATURE WINDING DESIGN UTILIZING HIGH-ORDER-HARMONICS

Based on the above analysis, main working harmonics of the traditional winding configuration are modulated from fundamental harmonic of DC field, whose PPNs can be expressed as follows:

$$P_w = \lvert N_p \pm N_r \rvert \tag{7}$$

where N_r is the number of salient rotor poles. Working harmonics of the novel winding configuration are modulated from high-order harmonic of DC field.

Different from working harmonics modulated from fundament harmonics of DC field, the working harmonics modulated from high order harmonics featured higher gear ratios, whose PPN can be expressed as follows:

$$P_w^{'} = \lvert kN_p \pm N_r \rvert \quad k = 3,5,7\ldots \tag{8}$$

It is found that modulated by stator teeth, there is abundant of fifth-order harmonic in the air-gap flux density, which indicates k=5 in the proposed motor with 18/13 slot/pole combination. [13]

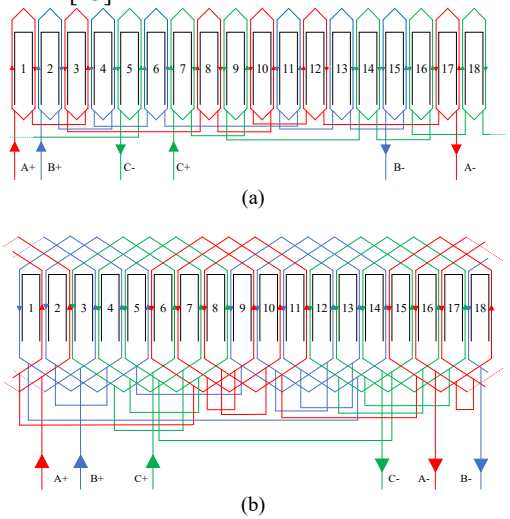

Fig. 5. Connections of ac armature winding. (a) Model I. (b) Model II.

Fig. 5 depicts the detailed connections of both winding designs. As shown in Fig.5, the concentrated over-lapped winding is adopted in Model I, and the slot pitch of the proposed distributed winding equals to 4 in Model II.

The reasonability of the proposed winding design can be explained by the ratio of flux density amplitudes of the two winding design's working harmonics mentioned above. From equation (6), the working harmonics consist of harmonics modulated from fundamental and higher harmonics. For the winding distribution of Model I, its main working harmonic selection is the component modulated from the fundamental dc field harmonic ($P_w = \lvert N_p - N_r \rvert = 10$). While for Model II, its main working harmonic is selected from the harmonic component modulated from the fifth order DC current field harmonics ($P^{'} = \lvert 5N_p - N_r \rvert = 2$). Then the ratio of the flux density amplitudes of these two working harmonics can be calculated from equation (6),

$$\left\lvert \frac{B_{(1,-1)}}{B_{(5,-1)}} \right\rvert = \left\lvert \frac{F_1 P_1}{F_5 P_1} \right\rvert = \left\lvert \frac{5\sin\left(\frac{N_p \theta_s}{2}\right)}{\sin\left(\frac{5N_p \theta_s}{2}\right)} \right\rvert \approx 1.34 \tag{9}$$

The calculation shows that the amplitude of the flux density of Model II is about 34% lower than the amplitude of Model I, but with much higher gear ratio. It can be calculated that, the gear ratio of the main working harmonics of Model I with conventional winding configuration is 1.3, while that of the main working harmonics of Model II equals to 6.5.

The angle difference of adjacent angle $\Delta\theta$ can be calculated as follows,

$$\Delta\theta = \frac{360P_w^{'}}{N_s} \tag{10}$$

According to the PPNs of main working harmonics of the two windings, $\Delta\theta$ of the proposed winding design is equal to 40deg, while that of the conventional winding equals to 100deg. The winding factor k_w of these two models are also calculated as following (11),

$$\begin{cases} k_w = k_d k_p \\ k_d = \left\lvert \frac{\sin\left(qn\frac{\alpha}{2}\right)}{q\sin\left(n\frac{\alpha}{2}\right)} \right\rvert \\ k_p = \sin\left(\frac{y}{\tau}\frac{\pi}{2}\right) \end{cases} \tag{11}$$

where k_p is the pitch factor, k_d is the distributed factor, q is the number of the least EMF vector per phase, n is the pole-pair number, α is the phasor angle between the neighboring coils.

TABLE III WINDING FACTOR COMPARISON

Parameters	Model I	Model II
Number of stator slots, N_s	18	18
Number of rotor slots, N_r	13	13
Winding design	conventional	proposed
Coil pitch	1 slot	4 slots
Pole pitch	1.8 slots	4.5 slots
Slot angle, α	100 deg	40 deg
Pitch factor, k_p	0.766	0.9848
Distribution factor, k_d	0.9598	0.9598
Winding factor, k_w	0.7352	0.9452

Thus, the armature winding design with winding pole pitch equals to 4 slots can be adopted. Thus, the concentrated

Authorized licensed use limited to: University of York. Downloaded on May 30,2023 at 13:00:08 UTC from IEEE Xplore. Restrictions apply.
© 2023 IEEE. Personal use is permitted, but republication/redistribution requires IEEE permission. See https://www.ieee.org/publications/rights/index.html for more information.

This article has been accepted for publication in IEEE Transactions on Magnetics. This is the author's version which has not been fully edited and content may change prior to final publication. Citation information: DOI 10.1109/TMAG.2023.3279887

over-lapped winding can also be adopted but will have lower winding factor that the proposed armature winding design.

The results for the models in this paper is shown in the Table III. The result shows that due to the proposed armature winding design utilizing the fifth-order harmonics in the air-gap exhibits higher winding factor than the conventional armature winding design, which implies the improvement of the power density of the motor.

IV. Performance Comparison

A. Air-gap flux density

In order to verify the theory of the second part, the finite element analysis (FEA) model of the motor is built with the parameters listed in Table I. The air-gap flux density of the motor at no load is calculated and analyzed in Fig.6. The result shows that due to the modulation of the stator tooth and rotor poles, there are a lot of space harmonic components in the air-gap, including the 2nd, 10th, 16th, 28th and so on.

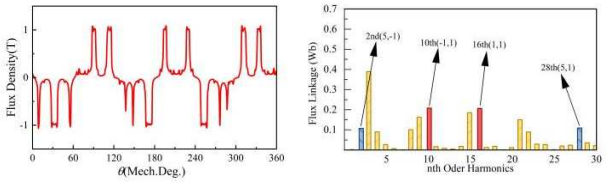

(a) (b)

Fig. 6. Flux density in the air-gap at no-load. (a) Waveform. (b) Spectrum.

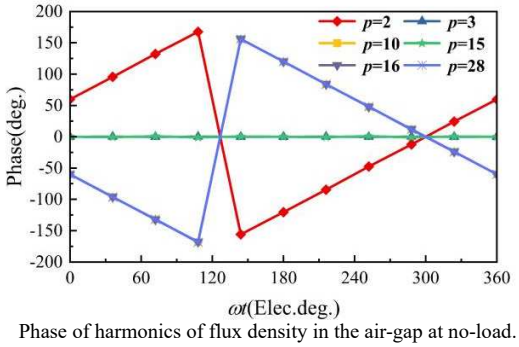

Fig. 7. Phase of harmonics of flux density in the air-gap at no-load.

The phase of the air gap harmonics is calculated and analyzed as Fig.7. As can be seen from the graph, the harmonics whose order equal to nN_p remain stationary because these harmonics do not go through the modulation of the rotor. The other four harmonics travel through an electrical cycle over one rotor tooth.

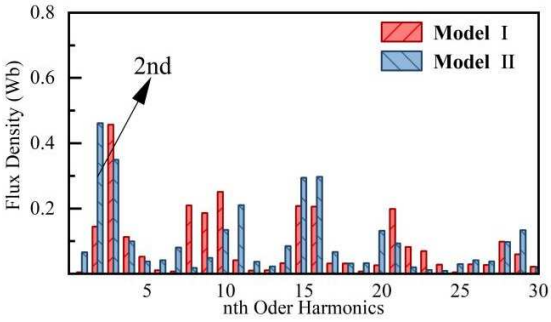

Fig. 8. Amplitude of harmonics of flux density in the air-gap at on-load.

The on-load air-gap flux density is also analyzed as shown in Fig.8 to verify the working harmonics of both armature winding design. The figure shows that the harmonics whose order is 2nd in the air-gap magnetic field are utilized using the proposed distributed armature winding with its amplitude much higher than that in the model with conventional concentrated armature winding design. The result of no-load and on-load air-gap flux density is consistent with the analysis in the Section II.

B. Back EMF

From the flux modulation theory, the 2nd harmonic's rotation speed is larger than that of the 10th harmonic. Therefore, the Model II with higher amplitude of the 2nd harmonic will produce higher back EMF at no load. The two models were analyzed using the FEA, and the results are shown in the Fig.9. As shown in Fig. 9, the amplitude of the back-EMFs of Model II is about 93% higher than that of Model I, which is in accordance with the theoretical derivation above. The 3D simulation result of Model II is also shown in the figure, which agrees well with the 2D result.

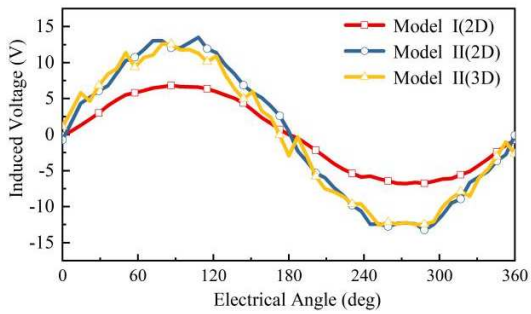

Fig. 9. Comparison of phase back EMF waveforms.

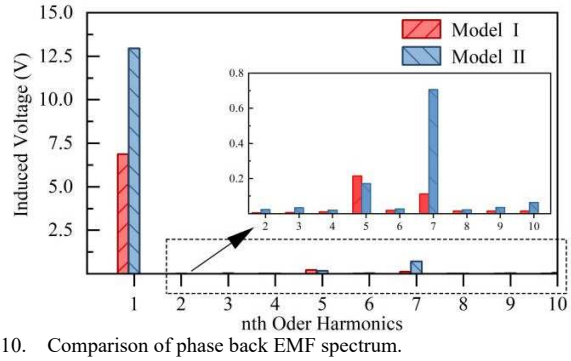

Fig. 10. Comparison of phase back EMF spectrum.

According to the results of the Fast Fourier Transformation (FFT) of the back EMF waveform, the fundamental harmonic's amplitude of Model II with the proposed winding is significantly increased due to the utilization of the high-order-harmonics in air-gap. Although the motor with the novel winding increases the harmonic amplitude of the specific number of back EMF waveform, such as 5th, 7th and 10th, they are too small to be negligible when compared with the amplitude of the fundamental harmonic.

C. Torque performance

The cogging torque of the model with concentrated winding and proposed distributed armature winding design are shown

Authorized licensed use limited to: University of York. Downloaded on May 30,2023 at 13:00:08 UTC from IEEE Xplore. Restrictions apply.
© 2023 IEEE. Personal use is permitted, but republication/redistribution requires IEEE permission. See https://www.ieee.org/publications/rights/index.html for more information.

This article has been accepted for publication in IEEE Transactions on Magnetics. This is the author's version which has not been fully edited and content may change prior to final publication. Citation information: DOI 10.1109/TMAG.2023.3279887

in Fig. 11. The cogging torque's amplitude are much smaller than their corresponding average torque.

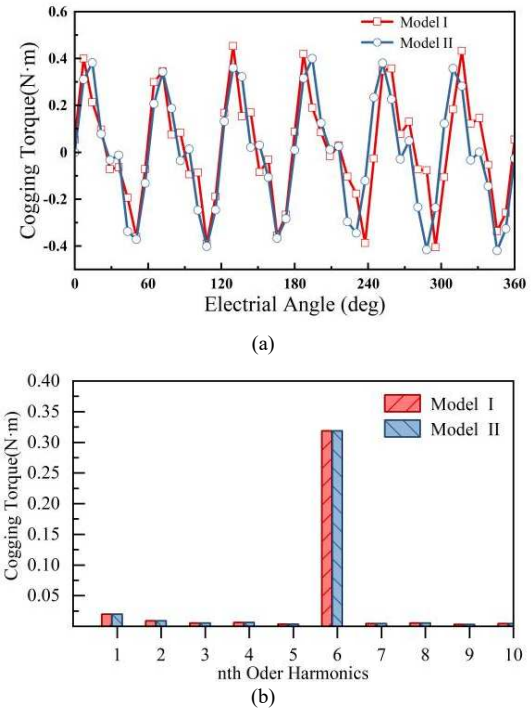

Fig. 11. Comparison of the cogging torque. (a) Waveform. (b) Spectrum.

The electromagnetic torques at full load of rated current density are compared in Fig. 13. As shown in Fig.13. Model II exhibits 54% higher torque. Due to the increased harmonics content in the induced voltage, the torque ripple of the machine with proposed winding configuration is also boosted. This can be furtherly suppressed by skew method. The 3D simulation result of Model II is also shown in the figure, which agrees well with the 2D result.

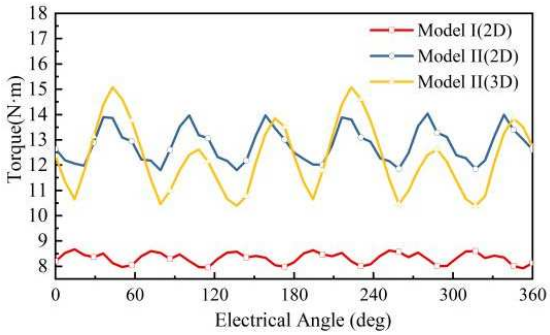

Fig. 12. Comparison of torque.

TABLE IV PERFORMANCE COMPARISON OF TWO MOTORS

Parameters	Model I	Model II
Winding design	Concentrated	Short-Pitch Distributed
Rated average torque (Nm), T_{avg}	8.3	12.8
Torque ripple (%) R_t	8.9%	17%
Torque Density (Nm/L), D	3.3	5.1
Maximum torque (Nm), T_{max}	13.4	16.3
Efficiency (@1200rpm) (%),η	86%	80%

In order to further analyze the characteristics of the motor, the overload performances of the motors are also calculated, whose current densities vary from 0A/mm^2 to 12A/mm^2 and the results are shown in the Fig.14. The simulation results show that the Model II saturates more easily than the Model I, but has a larger torque output at the same current density even when the current is three times of the rated current. TABLE IV summarizes the output torque performance of the two models.

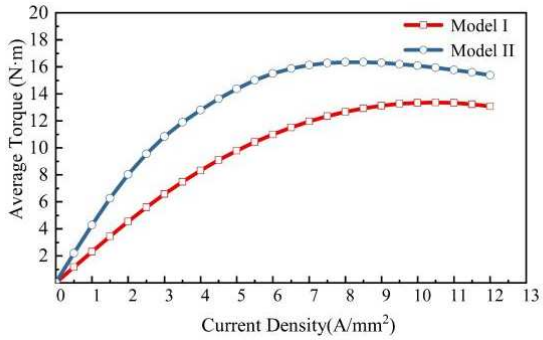

Fig. 13. Overload performance of the two machines.

V. CONCLUSION

In this paper, the flux modulation theory is introduced into a electrically excited doubly salient variable reluctance machine for armature winding design. The novel armature winding connection method for 18s/13r DC-DSVRM is based on the working harmonics modulated from the high-order harmonic of DC fields.

It was revealed that there is rich content of fifth-order harmonic in the MMF of DC field excitation. Thus, it is reasonable to choose working harmonic modulated from this high-order MMF for its higher gear ratio. The proposed armature winding configuration is designed according to the pole pair number which equals to $|5N_p - N_r|$ using distributed winding method. Two models with the same stator/rotor slots, external dimensions, field winding configuration and loading are compared in this paper to verify the merits of the proposed armature winding design., The simulation shows that the machine with novel distributed windings exhibits a 93% higher back EMF as well as 54% higher generated torque compared to an existing machine with conventional concentrated armature winding design under the same excitation condition.

Acknowledgement

This work was supported by the Research Grant Council of the Hong Kong Government under Project PolyU 152109/20E.

REFERENCES

[1] S. Niu, S. Wang and X. Zhao, "Overview of Stator Slot-Opening Permanent Magnet Machines," in IEEE Transactions on Transportation Electrification, vol. 9, no. 1, pp. 782-804, March 2023, doi: 10.1109/TTE.2022.3198438.

[2] Z. Li, X. Zhao and S. Niu, "Novel High-Order-Harmonic Toroidal Winding Design Approach for Double-Sided Vernier Reluctance Linear Machine," in *IEEE Transactions on Industrial Electronics*, pp. 1-11, 2022.

[3] S. Zheng, X. Zhu, L. Xu, Z. Xiang, L. Quan and B. Yu, "Multi-Objective Optimization Design of a Multi-Permanent-Magnet Motor Considering Magnet Characteristic Variation Effects," in IEEE Transactions on

Authorized licensed use limited to: University of York. Downloaded on May 30,2023 at 13:00:08 UTC from IEEE Xplore. Restrictions apply.
© 2023 IEEE. Personal use is permitted, but republication/redistribution requires IEEE permission. See https://www.ieee.org/publications/rights/index.html for more information.

This article has been accepted for publication in IEEE Transactions on Magnetics. This is the author's version which has not been fully edited and content may change prior to final publication. Citation information: DOI 10.1109/TMAG.2023.3279887

Industrial Electronics, vol. 69, no. 4, pp. 3428-3438, April 2022, doi: 10.1109/TIE.2021.3073311.

[4] Y. Du et al., "Comparison of Flux-Switching PM Motors With Different Winding Configurations Using Magnetic Gearing Principle," in IEEE Transactions on Magnetics, vol. 52, no. 5, pp. 1-8, May 2016, Art no. 8201908, doi: 10.1109/TMAG.2015.2513742.

[5] Q. Lin, S. Niu and W. Fu, "Design and Optimization of a Reluctance-Torque-Assisted Synchronous Motor with High Efficiency and Low Torque Ripple," 2019 22nd International Conference on Electrical Machines and Systems (ICEMS), Harbin, China, 2019, pp. 1-4, doi: 10.1109/ICEMS.2019.8922145.

[6] Z. Yang, F. Shang, I. P. Brown and M. Krishnamurthy, "Comparative Study of Interior Permanent Magnet, Induction, and Switched Reluctance Motor Drives for EV and HEV Applications," in IEEE Transactions on Transportation Electrification, vol. 1, no. 3, pp. 245-254, Oct. 2015, doi: 10.1109/TTE.2015.2470092.

[7] S. Jia, R. Qu, J. Li and Y. Chen, "Comparison of stator DC-excited vernier reluctance machines with synchronous reluctance machines," 2015 IEEE International Electric Machines & Drives Conference (IEMDC), Coeur d'Alene, ID, USA, 2015, pp. 649-655, doi: 10.1109/IEMDC.2015.7409128.

[8] S. Jia, R. Qu and J. Li, "Analysis of the Power Factor of Stator DC-Excited Vernier Reluctance Machines," in IEEE Transactions on Magnetics, vol. 51, no. 11, pp. 1-4, Nov. 2015, Art no. 8207704, doi: 10.1109/TMAG.2015.2450493.

[9] S. Jia, K. Yan, D. Liang and J. Liu, "Research on the Reactive Power Regulation Capability of Stator DC Current Excited Vernier Reluctance Machine," 2019 22nd International Conference on Electrical Machines and Systems (ICEMS), Harbin, China, 2019, pp. 1-5, doi: 10.1109/ICEMS.2019.8921936.

[10] D. Thyroff and I. Hahn, "Investigation of an Electrically Excited Vernier Machine with a Concentrated Winding intended for Traction Applications," 2019 26th International Workshop on Electric Drives: Improvement in Efficiency of Electric Drives (IWED), Moscow, Russia, 2019, pp. 1-5, doi: 10.1109/IWED.2019.8664396.

[11] L. Huang, Z. Q. Zhu, J. Feng, S. Guo and J. X. Shi, "Comparative Analysis of Variable Flux Reluctance Machines With Double- and Single-Layer Concentrated Armature Windings," in IEEE Transactions on Industry Applications, vol. 55, no. 2, pp. 1505-1515, March-April 2019, doi: 10.1109/TIA.2018.2884608.

[12] W. Wang, X. Zhao, S. Niu and W. Fu, "Comparative Analysis and Optimization of Novel Pulse Injection Sensorless Drive Methods for Fault-Tolerant DC Vernier Reluctance Machine," in IEEE Transactions on Power Electronics, vol. 37, no. 11, pp. 13566-13576, Nov. 2022, doi: 10.1109/TPEL.2022.3182054.

[13] X. Zhao, S. Wang, S. Niu, W. Fu and X. Zhang, "A Novel High-Order-Harmonic Winding Design Method for Vernier Reluctance Machine With DC Coils Across Two Stator Teeth," in *IEEE Transactions on Industrial Electronics*, vol. 69, no. 8, pp. 7696-7707, Aug. 2022.

[14] L. Jing, W. Liu, W. Tang and R. Qu, "Design and Optimization of Coaxial Magnetic Gear With Double-Layer PMs and Spoke Structure for Tidal Power Generation," in IEEE/ASME Transactions on Mechatronics, doi: 10.1109/TMECH.2023.3261987.

[15] L. Jing, W. Tang, T. Wang, T. Ben and R. Qu, "Performance Analysis of Magnetically Geared Permanent Magnet Brushless Motor for Hybrid Electric Vehicles," in IEEE Transactions on Transportation Electrification, vol. 8, no. 2, pp. 2874-2883, June 2022, doi: 10.1109/TTE.2022.3151681.

Authorized licensed use limited to: University of York. Downloaded on May 30,2023 at 13:00:08 UTC from IEEE Xplore. Restrictions apply.
© 2023 IEEE. Personal use is permitted, but republication/redistribution requires IEEE permission. See https://www.ieee.org/publications/rights/index.html for more information.